Experimental determination of effective light transport properties in fully anisotropic media

Research Article

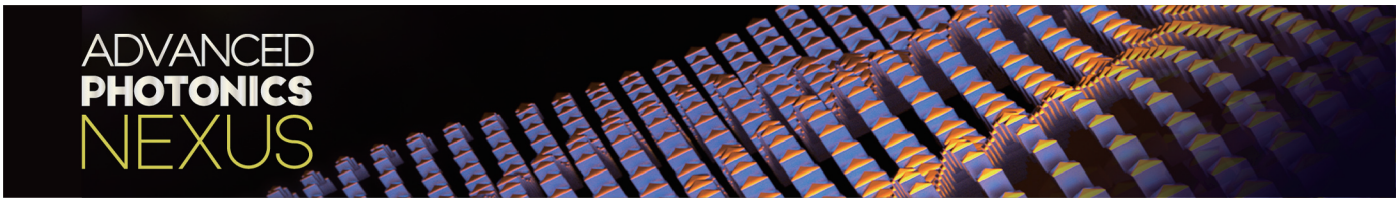

Experimental determination of effective light transport properties in fully anisotropic media

Ernesto Pini,[a,b,*] Peter Naglič,[c] Miran Bürmen,[c] Alexander Gatto,[d] Henrik Schäfer,[d] Diederik S. Wiersma,[a,b,e] and Lorenzo Pattelli[b,e,f,*]

[a]Università di Firenze, Department of Physics and Astronomy, Sesto Fiorentino, Italy
[b]European Laboratory for Non-Linear Spectroscopy, Sesto Fiorentino, Italy
[c]University of Ljubljana, Faculty of Electrical Engineering, Laboratory of Imaging Technologies, Ljubljana, Slovenia
[d]Sony Europe B.V., Stuttgart Technology Center, Stuttgart, Germany
[e]Istituto Nazionale di Ricerca Metrologica, Turin, Italy
[f]National Research Council – National Institute of Optics, Sesto Fiorentino, Italy

Abstract. Structurally anisotropic materials are ubiquitous in several application fields, yet their accurate optical characterization remains challenging due to the lack of general models linking their scattering coefficients to the macroscopic transport observables and the need to combine multiple measurements to retrieve their direction-dependent values. Here, we present an improved method for the experimental determination of light-transport tensor coefficients from the diffusive rates measured along all three directions, based on transient transmittance measurements and a generalized Monte Carlo model. We apply our method to the characterization of light-transport properties in two common anisotropic materials—polytetrafluoroethylene tape and paper—highlighting the magnitude of systematic deviations that are typically incurred when neglecting anisotropy.

Keywords: multiple scattering; time-resolved transmittance; anisotropic diffusion; scattering tensor; optical gating; fibrous materials.

Received May 20, 2024; revised manuscript received Jul. 1, 2024; accepted for publication Aug. 16, 2024; published online Sep. 12, 2024.

[DOI: 10.1117/1.APN.3.5.056017]

1 Introduction

Turbid media are encountered in several applied and fundamental research fields, where determining the light-transport properties of these materials is important to study their microscopic structure and composition.[1] Among several experimental techniques, time-domain methods are particularly useful, as they allow one to isolate contributions dominating at different time scales, ranging from early ballistic light to the late multiple scattering regime.[2,3] Despite the importance of an accurate determination of these properties, however, the experimental retrieval of scattering parameters is typically performed under the assumption that light transport is isotropic—even when the material under study is visibly anisotropic.[4–8] Ignoring the presence of anisotropic light transport clearly introduces an error in the determination of the microscopic scattering properties, the magnitude of which is currently not well characterized.

This bias can have important consequences for the characterization of tissues, fibrous materials, and strongly scattering media—which often exhibit an anisotropic structure or morphology. In the large majority of cases, the scattering strength of these materials has been characterized using a single (scalar) transport mean free path, which however can be quite far from the value of the actual components of their scattering tensor, and even from their direction-averaged value. In addition, the experimental methods that are used to infer a single mean free path value for an anisotropic medium are inevitably more sensitive to the scattering strength along a certain direction. Thus, whenever an anisotropic medium is characterized via a single scalar mean free path, the resulting value may be more or less indicative of the scattering properties in the plane[6,9–13] or those along the perpendicular direction,[4,5,7,14,15] rather than being representative of the whole medium.

*Address all correspondence to Ernesto Pini, ernesto.pini.unifi.it; Lorenzo Pattelli, l.pattelli@inrim.it

For isotropic materials, a simple relation exists linking the transport mean free path ℓ^* to the (experimentally observable) diffusive constant $D = v\ell^*/3$, with v as the energy velocity in the medium. At the microscopic level, this isotropic transport mean free path is in turn related to the scattering mean free path ℓ_s (defined as the inverse of the scattering coefficient $\ell_s = 1/\mu_s$) via a "similarity relation" $\ell^* = \ell_s/(1-g)$ involving the cosine of the average polar scattering angle g. Therefore, for an isotropic medium, the relation between the macroscopic observable diffusion rate and the microscopic scattering property can be written as

$$D = \frac{1}{3} v\ell^* = \frac{1}{3}\frac{v}{\mu_s'} = \frac{1}{3}\frac{v}{\mu_s(1-g)}, \tag{1}$$

with $\mu_s' = \mu_s(1-g)$ defined as the reduced scattering coefficient.

In anisotropic materials, however, all parameters of interest can in principle become 3×3 tensor quantities, including D, μ_s, g, and v. Assuming for simplicity that all tensors can be diagonalized in a common reference frame, one can still define the diagonal components of the scattering tensor as $\mu_{s,i} = 1/\ell_{s,i}$ and diffusive rate tensor as $D_i = v_i\ell_i^*/3$, with $i \in \{x, y, z\}$. In this case, however, the relation between the components of these tensors is not expected to follow the form of Eq. (1) anymore, exhibiting instead a more complex (and in general, unknown) dependence on the other coefficients. Analytical solutions have been derived recently in simplified anisotropic scenarios, showing how all tensor components contribute to determining the diffusion coefficient along a given direction.[16] In this work, we consider the more general case of fully anisotropic materials ($\mu_{s,x} \neq \mu_{s,y} \neq \mu_{s,z}$) with asymmetric scattering ($g \neq 0$) and a refractive index mismatch at the boundary, for which an analytical relationship may not exist altogether.

To elucidate this gap, multiple competing descriptions of anisotropic transport have been proposed in the past years,[17–21] which, however, do not provide a general link between microscopic scattering parameters and the corresponding diffusion observables. For this reason, a trade-off must be introduced that allows one to properly account for transport anisotropy while keeping the number of tensor quantities involved in the inverse problem to a minimum to allow their practical determination.

To improve on the current situation and avoid the use of oversimplified isotropic assumptions, we introduce a microscopic effective transport tensor and present a method to determine its components for scattering media with full anisotropy in all three spatial directions. To this purpose, we assume a tensor scattering coefficient μ_s while keeping the asymmetry factor g, absorption coefficient μ_a, and refractive index n as scalar quantities. This choice is motivated by multiple reasons. First, imposing the anisotropy only in the scattering coefficient avoids cross-talk effects between different tensors, which might result in the impossibility of uniquely determining the optical properties of an anisotropic sample. Second, a strategy for including a direction-dependent asymmetry factor is not established yet in the literature, with different proposals leading to different results.[9,17,22] Finally, using a scalar value of g allows one to define effective transport mean free path values $\tilde{\ell}_i^*$ in analogy with the standard similarity relation, as needed for materials characterized by a limited optical thickness or a strong forward scattering,

$$\tilde{\ell}_i^* = \frac{1}{\tilde{\mu}_{s,i}'} = \frac{1}{\mu_{s,i}(1-g)}. \tag{2}$$

Defining an effective transport mean free path is of practical utility when dealing with turbid samples, as it allows one to account for the transient effects due to scattering asymmetry while leaving the overall diffusion tensor D almost unaffected for small variations of g. This approach captures the key features of anisotropic transport, such as the expected discrepancy between the observed diffusive rates (expressed in units of length as transport mean free paths ℓ_i^*) and their effective microscopic counterparts $\tilde{\ell}_i^*$, which becomes more significant with increasing structural anisotropy. More fundamentally, it allows one to restore a link between a random walk description of transport and the resulting diffusive rates by assigning different identities to these two parameters.

We apply this approach to experimental measurements obtained using an optical gating technique[16,23–25] and analyze the results using a newly developed and open-source Monte Carlo (MC) package named PyXOpto,[26] which is capable of handling tensor scattering coefficients.

The paper is organized as follows: in Sec. 2, we start by commenting on the typical degree of apparent degeneracy that can be expected between isotropic and anisotropic transport by showing a few representative examples of time-domain transmittance through a slab geometry. Resorting to an isotropic model or theory in this configuration can lead to significant systematic errors even when time-resolved measurements are limited to the retrieval of scattering properties along the depth direction. Experimental and numerical methods are described in Sec. 3. Results are presented in Sec. 4 relative to the determination of the transport properties of two common laboratory materials, providing a quantitative illustration of the typical errors incurred when disregarding anisotropic light transport. Finally, conclusions and perspectives are drawn in Sec. 5.

2 Decay Rate Degeneracy

In many experimental configurations of interest, a slab sample is illuminated from the perpendicular direction to its interface, and the decay rate of the intensity transmitted or reflected from the sample interface is studied. This decay rate is determined by various properties of the sample: the refractive index contrast with the environment, the thickness of the slab, the absorption coefficient, and the diffusion coefficient along the perpendicular axis. At the microscopic level, however, the diffusion coefficient depends on the scattering properties along all directions,[16,19] meaning that it is not possible to reliably infer the scattering coefficient along the perpendicular direction from a time-domain measurement alone, even when all other properties are known.

To illustrate this issue, we consider a set of MC simulations showing that several different anisotropic configurations can give rise to transmittance decay rates that are degenerate with the isotropic case, despite using different scattering coefficients along the illumination direction z. Taking a nonabsorbing 1 mm-thick slab with isotropic scattering $\mu_{s,iso} = 10\ \text{mm}^{-1}$ and refractive index contrast of $n = 1$ or $n = 1.2$, one can find alternative configurations with predefined degrees of anisotropy (encompassing both cases of partial or full 3D anisotropy) that give rise to the same transmittance decay rate (Fig. 1).

Despite the different scattering coefficients, the resulting curves are nearly identical except for a constant scaling factor and the initial transient. Experimentally, these differences are not decisive enough to tell isotropic samples apart from anisotropic

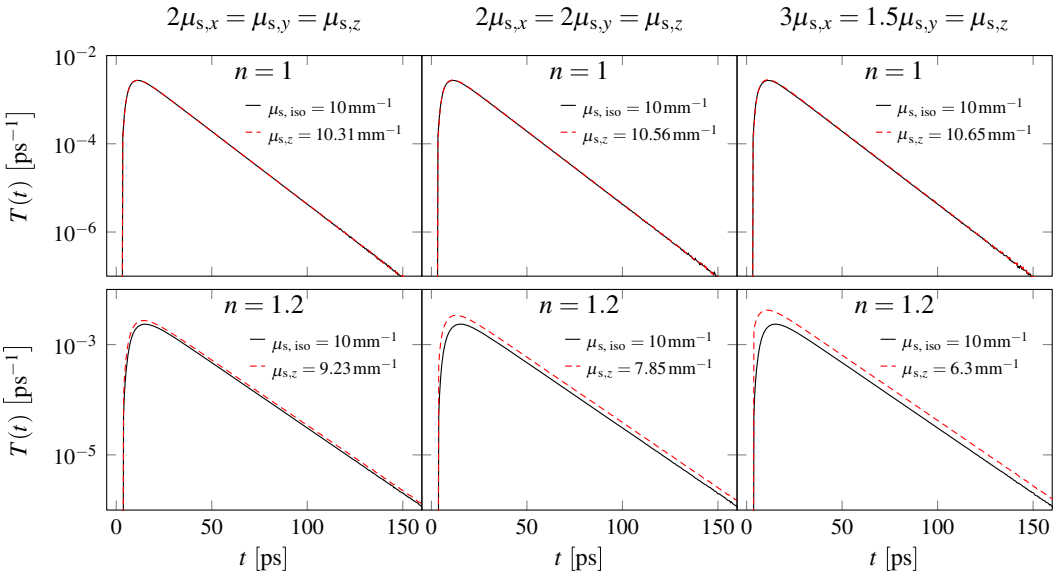

Fig. 1 Time-resolved transmittance $T(t)$ through a nonabsorbing 1 mm-thick scattering slab for two refractive index contrast values $n = 1, 1.2$. Solid curves represent isotropic simulations with $\mu_{s,iso} = 10$ mm^{-1}. For each case, a predefined ratio between scattering coefficients along different axes is imposed, as specified in the title above each column. Anisotropic configurations exhibiting the same decay rate as the isotropic case are shown, leading to values of $\mu_{s,z} \neq \mu_{s,iso}$. All simulations are performed setting $g = 0$.

samples, since time-resolved curves are typically measured with arbitrary units, and the details of the early transient are often concealed by the finite duration of the illumination pulse. For the representative configurations shown here, deviations between the isotropic scattering coefficient $\mu_{s,iso}$ and the longitudinal one $\mu_{s,z}$ range from a few percent in the index-matched cases, up to 37% in the presence of full 3D anisotropy and moderate refractive index contrast. Notably, in general these deviations can both over- or under-estimate the true $\mu_{s,z}$, depending on the values of the scattering coefficients along the other directions, the refractive index contrast, and the optical thickness of the slab. It should be further noted that if the absorption coefficient is also unknown and left as a free parameter, almost perfect degeneracy among all curves can be typically obtained at all times, since in this case the extra multiplicative degree of freedom $e^{-\mu_a vt}$ can be used to independently tune the decay rate, casting an even larger deviation on the scattering properties of anisotropic media retrieved using isotropic models.

These examples show that, for any practical purposes, time-resolved curves alone have limited informative value for the study of structurally anisotropic media and need to be complemented by additional independent measurements. This is particularly problematic when anisotropy is disregarded and transmittance measurements are fitted with an isotropic model.

3 Materials and Methods

3.1 Experimental Setup

We approach the study of anisotropic materials using an experimental setup based on the transient imaging optical gating method, which is capable of providing both spatial and time-domain information on the evolution of intensity profiles.[23,24] A Ti:Sa laser source generates a train of pulses at a wavelength of 820 nm with an 80 MHz repetition rate and a typical duration of about 150 fs. Each pulse goes through an optical parametric oscillator resulting in two synchronous outputs with different wavelengths: a residual of the original pulse at 820 nm and a converted pulse at 1525 nm [Fig. 2(a)]. In the experiment, a motorized stage is used to adjust the relative delay between the two laser beams, which can either serve as the probe or the gate arms of the setup. The probe beam is focused on the sample down to a focal spot of 30 μm to generate a diffused transmittance signal, which is then recombined with the gate beam in a collinear fashion onto a β-barium borate (BBO) crystal. A sum-frequency signal is finally generated at a wavelength of 533 nm, proportional to the cross-correlation amplitude between the diffuse transmittance and the gate pulse at a given delay. The gate beam is expanded to achieve a uniform intensity distribution over the whole nonlinear crystal surface to obtain an accurate conversion of the signal spatial distribution. Unconverted residues of the two infrared beams are filtered out by a series of short-pass and bandpass filters.

The resulting upconverted time-resolved signal can be then either integrated by a photomultiplied detector or resolved spatially with a CCD camera recording the transient intensity profiles transmitted through the scattering medium. Due to the spatially uniform upconversion efficiency guaranteed by the expanded and collinear gate beam, the generated images provide quantitative information on the transverse propagation light at the exit surface of the sample, from which the diffusive rates along different directions can be estimated directly. All measurements are averaged over multiple sample positions in an area of $\sim$4 mm^2 to reduce fluctuations due to small local inhomogeneities and speckle patterns.

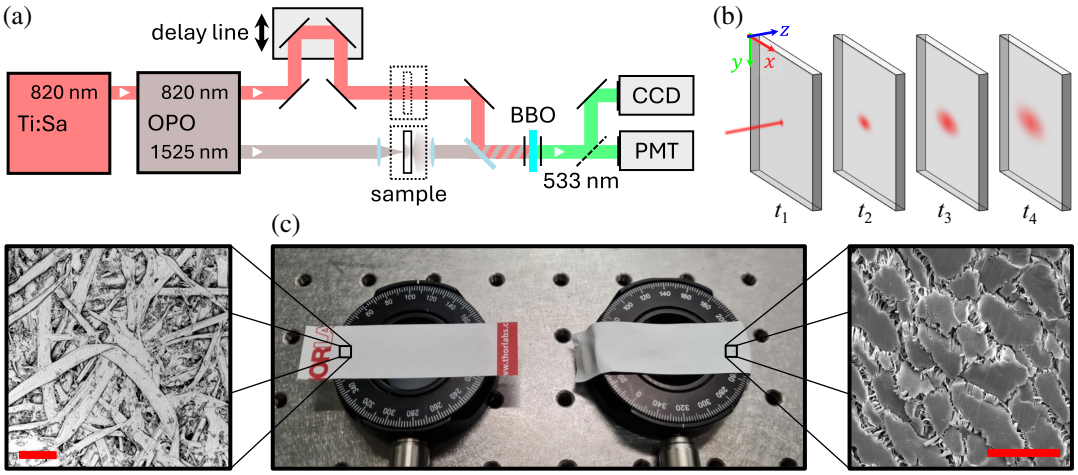

Fig. 2 (a) Sketch of the experimental setup for time-resolved measurements when using a 1525 nm probing wavelength. Ti:Sa, titanium sapphire fs laser; OPO, optical parametric oscillator; BBO, β-barium borate nonlinear crystal; CCD, charge-coupled device camera; PMT, photomultiplier tube. (b) Schematics of the transient imaging measurement on a slab sample. The instantaneous spatial distribution of transmitted intensity is imaged at different time delays. (c) Photograph of the paper Post-it note (left) and PTFE tape strip (right) with corresponding scanning electron microscope images of the two samples (insets). Scale bars correspond to 100 and 30 μm for paper and PTFE tape, respectively.

3.2 Data Analysis and MC Simulations

Intensity profiles are recorded at different time delays, as exemplified in Fig. 2(b). The profiles are rotated for convenience to align the intrinsic sample anisotropy axes to the laboratory reference frame and then fitted with bivariate Gaussian distributions to retrieve the instantaneous mean square displacement (MSD) along the y (vertical) and x (horizontal) axes. The spread rate of the intensity profiles provides direct access to the x and y diffusion rates, independent of any absorption contribution.[2,16] Thus, performing a linear regression on the MSD evolution after the initial transient allows one to retrieve the diffusive constants D_x, D_y, which are proportional to the corresponding slopes. Information on the diffusive rate along z (and the absorption coefficient μ_a) is finally extracted by integrating the total transmitted intensity in each frame or using a photomultiplier tube for convenience.

In order to retrieve the microscopic scattering coefficients associated with the observed diffusive rates, anisotropic MC simulations are performed by varying the scattering coefficient tensor components until the experimental MSD growth and the time-resolved transmittance curves are simultaneously reproduced with a single simulation. To this purpose, we used the PyXOpto open-source implementation of the MC method, which is capable of handling tensor scattering properties.[26] In the fitting procedure, the three components of the scattering tensor $\mu_{s,x}$, $\mu_{s,y}$, and $\mu_{s,z}$ are used as independent free parameters, plus a scalar asymmetry factor g that is applied to all three axes.

4 Results

We characterize light transport experimentally in two common materials: polytetrafluoroethylene (PTFE) (Teflon) tape and paper, both of which are generally known for their highly anisotropic structure and vanishing absorption at visible and near-infrared wavelengths. Notably, paper and PTFE tape are also commonly indicated as reference diffusers in the evaluation protocols for the temporal performance of near-infrared spectroscopy applications, based on the assumption that they contribute negligibly to the temporal dispersion of the illumination pulse.[27] However, to the best of our knowledge, the transport mean free path in these materials is not known precisely, as previous time-resolved measurements were unable to appreciate their multiple scattering regimes.[28]

In the following, we perform time-domain transmittance measurements through these samples and analyze the results using both isotropic and anisotropic MC simulations, which allows us to determine the magnitude of the error introduced by not accounting properly for the structural anisotropy of the materials.

4.1 PTFE Tape

The first sample we consider is a strip of Teflon tape commonly used for sealing pipe threads. Teflon tape is made by PTFE fibers exhibiting a preferential alignment, which endows it with a marked structural anisotropy. This anisotropy affects also light-transport properties, as confirmed by previous reports on the observation of direction-dependent light diffusion in this material.[29,30]

We measure the transmittance through a freestanding strip of tape at a probe wavelength of 1525 nm. The tape sample is attached on a rotating mount to allow its alignment with the laboratory reference frame [Fig. 2(c)] and verify that the elongated transmittance profiles rotate integrally with the sample. The analysis reveals the presence of a direction of faster diffusion at an angle of ~45 deg with respect to the direction of the tape strip. This angle corresponds to the direction perpendicular to the alignment of the PTFE fibers, as determined by scanning electron microscopy images, in agreement with previous

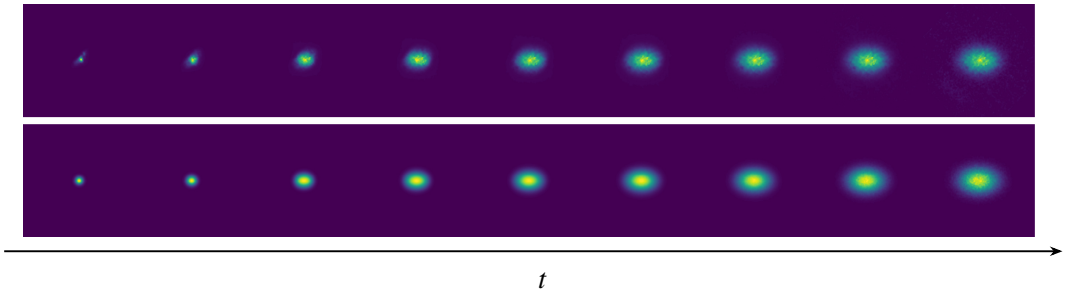

Fig. 3 Selection of transient imaging measurements (top) and corresponding best-fit MC simulations (bottom) of the transmitted intensity distribution recorded at different times for the PTFE tape sample probed at 1525 nm. Each frame shows an area of 7.4 mm × 7.4 mm and is normalized to its maximum intensity value. The time delay between consecutive frames is $\Delta t = 1.33$ ps.

reports.[29] Closer inspection of the electron microscopy picture shows that the polymer fibers have a flattened shape along the main plane of the tape and are further fused together to form planar flakes on its external surface. This morphology suggests that different scattering coefficients could be found along each direction, resulting in a fully anisotropic sample.

The main set of transient imaging measurements was performed in a fixed orientation configuration (Fig. 3), rotated so that the faster axis of diffusion coincides with the x axis in the laboratory reference frame. An average refractive index of $n = 1.05$ was evaluated for the slab using the Bruggeman mixing rule[31] based on the PTFE/air volume fraction estimated by a weighting method. Sample thickness was set to $L = 200$ μm, as directed by the tape manufacturer. The diffusion coefficients can be derived directly with a linear regression on the MSD evolution after the initial transient for x and y [Fig. 4(a)], returning values of $D_x = (289 \pm 7) \times 10^2$ μm^2 ps^{-1} and $D_y = (117 \pm 2) \times 10^2$ μm^2 ps^{-1}.

The resulting best-fit MC simulation is in excellent agreement with both the MSD evolution and the time-resolved transmitted intensity, reproducing also finer experimental features such as the initial acceleration and subsequent slowing down of the fast-axis MSD growth [Fig. 4(a)], or the more prominent transmittance peak at $t \sim 1$ ps [Fig. 4(b)].

The corresponding effective transport mean free path values are $\tilde{\ell}_x^* = (210 \pm 20)$ μm, $\tilde{\ell}_y^* = (95 \pm 7)$ μm, and $\tilde{\ell}_z^* = (130 \pm 14)$ μm, which remain basically unaltered when forcing different values of g around its fitted value of 0.9.

It is interesting to note that the ratio between the diffusive constants $D_x/D_y = 2.47$ is appreciably different from the ratio between the effective transport mean free paths $\tilde{\ell}_x^*/\tilde{\ell}_y^* = 2.21$, which confirms the different roles taken by these two parameters and shows that a direct measurement of the diffusion dynamics does not even provide relative information on the microscopic degree of anisotropy due to the nontrivial mixing of the scattering coefficients along all directions.

An attempt to fit the time-resolved experimental data is also performed assuming an isotropic MC model, using the previously determined values for n, μ_a, and g, with $\mu_{s,iso}$ as the only free parameter. The result shows a comparable agreement [Fig. 4(b)], returning, however, a value that differs by 24% from the actual scattering coefficient along the z axis, as summarized in Table 1.

4.2 Paper

The second anisotropic sample that we study is a piece of common paper, which is a material known for its structural

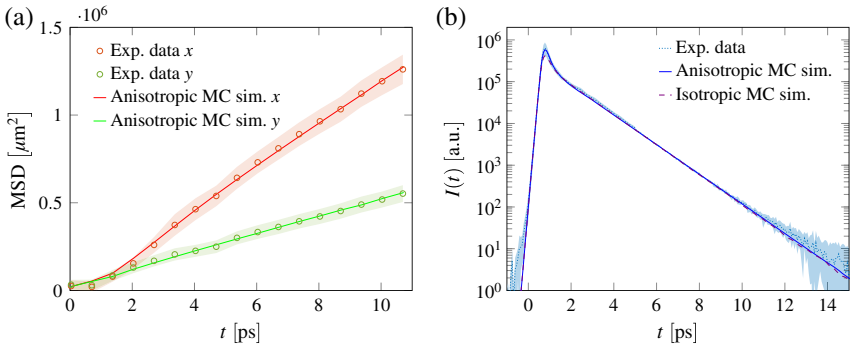

Fig. 4 (a) MSD and (b) time-resolved transmitted intensity of PTFE tape. Solid lines represent the best-fit anisotropic MC simulations, obtained with $\mu_{s,x} = 48$ mm^{-1}, $\mu_{s,y} = 105$ mm^{-1}, $\mu_{s,z} = 77$ mm^{-1}, $g = 0.9$, and $\mu_a = 0$. The dashed purple curve shows a fit performed with an isotropic MC simulation with $\mu_{s,iso} = 95$ mm^{-1}. Shaded areas represent (a) the compounded uncertainty from the pixel-to-micrometer conversion and the bivariate Gaussian fit and (b) 1σ of the average between five different sample positions, respectively.

Table 1 Effective transport mean free paths $\tilde{\ell}_i^*$ along different directions retrieved with anisotropic MC simulations for PTFE tape and paper. The transport mean free paths retrieved with isotropic MC modeling (ℓ_{iso}^*) are also reported to show the degree of error introduced by neglecting the presence of anisotropy.

Sample	$\tilde{\ell}_x^*$ [μm]	$\tilde{\ell}_y^*$ [μm]	$\tilde{\ell}_z^*$ [μm]	ℓ_{iso}^* [μm]
PTFE	210(20)	95(7)	130(14)	105(13)
Paper	22.4(1.8)	34(3)	14.6(1.7)	11(1)

anisotropy arising from the preferential alignment of its cellulose fibers imparted during its industrial fabrication process.[32–34] A Post-it note was tested in a transmission configuration at a probing wavelength of 820 nm, aligning the fast diffusion direction along the y axis (Fig. 5).

Sample thickness was determined by directly measuring a stack of 50 Post-it notes using a precision micrometer, yielding a value of $L = (100 \pm 5)$ μm, while its effective refractive index was evaluated at $n = 1.25$ using the same method applied for the PTFE tape. In contrast with the previous case, a small but measurable absorption coefficient was detected and independently confirmed at a value of $\mu_a = 0.015$ mm^{-1} by an additional time-resolved reflectance measurement by a thick stack of Post-it notes. This value was used in the subsequent analysis, together with a value of $g = 0.8$, in agreement with previous estimates in the literature.[35,36] The diffusive coefficients measured from the MSD growth rates [Fig. 6(a)] are $D_x = (18.8 \pm 1.1) \times 10^2$ μm^2 ps^{-1} and $D_y = (26 \pm 2) \times 10^2$ μm^2 ps^{-1}, where the larger uncertainty compared to the case of the PTFE tape is determined by the larger inherent inhomogeneity of paper, which exhibits slight density and thickness fluctuations at different positions.

As in the previous case, the resulting best-fit anisotropic model shows a good agreement with both the MSD evolution and the time-resolved measurement [Fig. 6(b)], excluding an initial transient affected by the local inhomogeneities at the illumination spot. The fit returned effective scattering mean free path values of $\tilde{\ell}_x^* = (22.4 \pm 1.8)$ μm, $\tilde{\ell}_y^* = (34 \pm 3)$ μm, and $\tilde{\ell}_z^* = (14.6 \pm 1.7)$ μm. A ratio of $D_y/D_x = 1.38$ is found between the diffusive coefficients, to be compared with a value of $\tilde{\ell}_y^*/\tilde{\ell}_x^* = 1.52$ for the corresponding effective mean free paths.

The best fit obtained using an isotropic MC model is also shown in Fig. 6(b), showing also in this case very good agreement at the cost of a 36% systematic error in the retrieved scattering coefficient. All fitted parameters are summarized in Table 1.

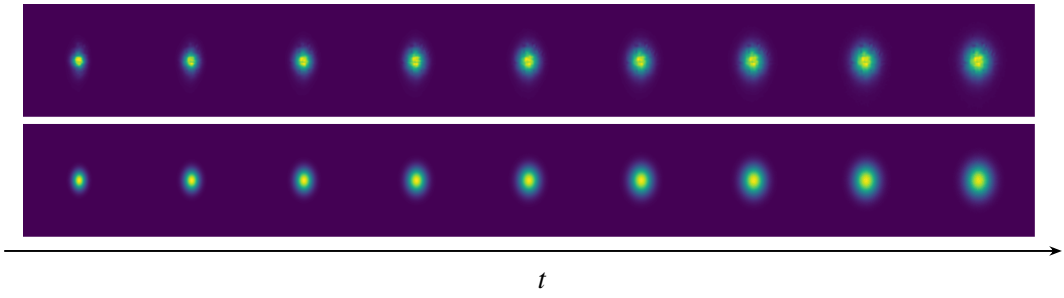

Fig. 5 Selection of transient imaging measurements (top) and corresponding best-fit MC simulations (bottom) of the transmitted intensity distribution recorded at different times for the Post-it note performed at 820 nm probing wavelength. Each frame shows an area of 2.7 mm × 2.7 mm and is normalized to its maximum value. The time delay between consecutive frames is $\Delta t = 1$ ps.

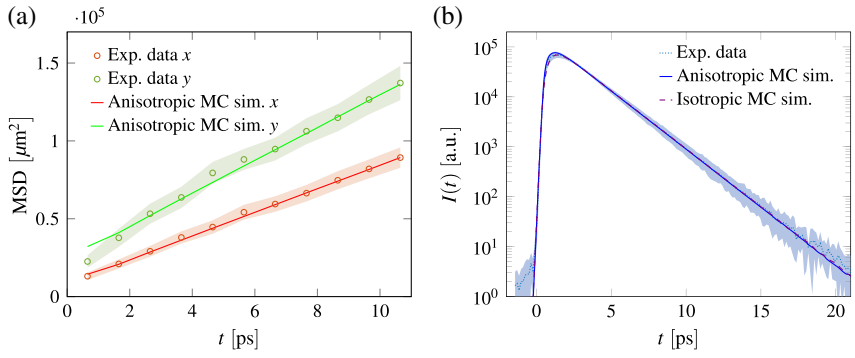

Fig. 6 (a) MSD and (b) time-resolved transmitted intensity of paper. Solid lines represent the best-fit anisotropic MC simulations, obtained with $\mu_{s,x} = 223$ mm^{-1}, $\mu_{s,y} = 148$ mm^{-1}, $\mu_{s,z} = 343$ mm^{-1}, $g = 0.8$, and $\mu_a = 0.015$ mm^{-1}. The dashed purple curve shows a fit performed with an isotropic MC simulation with $\mu_{s,\text{iso}} = 455$ mm^{-1}. Shaded areas represent (a) the compounded uncertainty from the pixel-to-micrometer conversion and the bivariate Gaussian fit and (b) 1σ of the average between six different sample positions, respectively.

5 Discussion and Conclusion

In this work, we presented optical gating as a versatile transient imaging method for the study of direction-dependent diffusion of light in structurally anisotropic materials. The experimental intensity profiles can be directly compared against the output of a general and open-source MC description of anisotropic light propagation to retrieve the full transport coefficient tensor of arbitrary anisotropic materials. We demonstrate our analysis for two common materials exhibiting different diffusive rates along each axis, showing how their time-resolved traces can be easily reproduced with either isotropic or anisotropic MC models. Due to the interplay among all components of the scattering tensor, assuming an isotropic model for an anisotropic material can lead to a substantial error in the determination of the true transport mean free path of a scattering sample, even when the measurement is intended to retrieve only the component along the normal direction to the sample interface. It is also interesting to note that, for the relatively thin samples studied here, the transport mean free path retrieved under the (incorrect) isotropic transport assumption is typically shorter than the direction-averaged value, and in the case of paper, even shorter than the shortest component of the corresponding anisotropic mean free path tensor.

Despite the significant advancement offered by new experimental techniques and numerical methods, the complete characterization of structurally anisotropic scattering materials presents still several open challenges. Significant cross talk is expected, for instance, when approaching the inverse problem for samples exhibiting anisotropic scattering coefficients combined with birefringence, tensor scattering asymmetry, or tensor absorption properties. This is commonly the case for several common materials, such as biological tissues[37–41] or liquid crystals[42,43]—which will likely require an even larger number of independent measurements to constrain the inverse problem associated with the accurate retrieval of their optical properties—but also for media presenting different orientations of their structural anisotropy at different locations, such as the brain,[44–46]teeth,[47,48] skin under mechanical deformation,[49,50] or sea ice.[51,52] On the other hand, the correct assessment of anisotropic light transport may also offer some opportunities for applications, e.g., in the ink-printing industry[53,54] or in the field of imaging through scattering media, where the narrower angular distributions associated with strongly anisotropic transport may introduce correlations similar to those found for strongly forward-scattering materials.[55]

Our results highlight the importance of taking into account the presence of structural anisotropy in scattering materials, and the need to investigate all directions rather than just planar or perpendicular propagation, as they all contribute to the determination of the actual transport mean free path along a direction of interest. In addition, we further evaluated the potential errors incurred when using an isotropic model for the interpretation of anisotropic transport data, which show a tendency to overestimate the true scattering strength in the case of turbid anisotropic materials. Notably, this approach has been often used for the characterization of highly scattering materials and their intercomparison in terms of scattering efficiency along the thickness direction, which calls for a careful reanalysis of previously published results in light of this potential systematic bias. To this purpose, the development of new scattering phantoms with controlled structural anisotropy is strongly needed for further validation of this interplay in samples with different anisotropic morphologies and to advance our understanding of how to correctly model materials where both the scattering coefficient and the scattering asymmetry factor are direction-dependent.

6 Disclosures

The authors declare no competing interests.

7 Code and Data Availability

All the data that support the findings of this study are available from the corresponding authors upon request. The code used for MC simulations is freely available at https://github.com/xopto/pyxopto.

Acknowledgments

This work was partially funded by the European European Union's NextGenerationEU Programme with the I-PHOQS Research Infrastructure [IR0000016, ID D2B8D520, CUP B53C22001750006] "Integrated infrastructure initiative in Photonic and Quantum Sciences." E.P. acknowledges financial support from Sony Europe B.V. L.P. acknowledges the CINECA award under the ISCRA initiative, for the availability of high-performance computing resources and support (ISCRA-C "ARTTESC"), and NVIDIA Corporation for the donation of the Titan X Pascal GPU. M.B. and P.N. acknowledge financial support from the Slovenian Research and Innovation Agency (Grant Nos. J2-2502, L2-4455, and J2-50092). Fabrizio Martelli is kindly acknowledged for the fruitful discussion.

References

1. F. Martelli et al., *Light Propagation through Biological Tissue and Other Diffusive Media: Theory, Solutions, and Validations*, SPIE Press, Bellingham, Washington (2022).
2. G. Mazzamuto et al., "Deducing effective light transport parameters in optically thin systems," *New J. Phys.* **18**(2), 023036 (2016).
3. T. Svensson et al., "Exploiting breakdown of the similarity relation for diffuse light transport: simultaneous retrieval of scattering anisotropy and diffusion constant," *Opt. Lett.* **38**(4), 437–439 (2013).
4. T. Strudley et al., "Mesoscopic light transport by very strong collective multiple scattering in nanowire mats," *Nat. Photonics* **7**(5), 413–418 (2013).
5. M. Burresi et al., "Bright-white beetle scales optimise multiple scattering of light," *Sci. Rep.* **4**(1), 6075 (2014).
6. K. Konagaya et al., "Optical properties of drying wood studied by time-resolved near-infrared spectroscopy," *Opt. Express* **24**(9), 9561–9573 (2016).
7. H. Yang et al., "Cellulose-based scattering enhancers for light management applications," *ACS Nano* **16**(5), 7373–7379 (2022).
8. M. Moradi and Y. Chen, "Monte Carlo simulation of diffuse optical spectroscopy from multi-layered semi-infinite turbid media for modeling dental tissues," *Sensors* **23**(11), 5118 (2023).
9. A. Kienle et al., "Determination of the optical properties of anisotropic biological media using an isotropic diffusion model," *J. Biomed. Opt.* **12**(1), 014026 (2007).
10. O. L. Muskens et al., "Large photonic strength of highly tunable resonant nanowire materials," *Nano Lett.* **9**(3), 930–934 (2009).
11. L. Cortese et al., "Anisotropic light transport in white beetle scales," *Adv. Opt. Mater.* **3**(10), 1337–1341 (2015).
12. M. Moffa et al., "Biomineral amorphous lasers through light-scattering surfaces assembled by electrospun fiber templates," *Laser Photonics Rev.* **12**(1), 1700224 (2018).

13. P. Krauter, C. Zoller, and A. Kienle, "Double anisotropic coherent backscattering of light," *Opt. Lett.* **43**(8), 1702–1705 (2018).
14. M. S. Toivonen et al., "Anomalous-diffusion-assisted brightness in white cellulose nanofibril membranes," *Adv. Mater.* **30**(16), 1704050 (2018).
15. W. Zou et al., "Biomimetic polymer film with brilliant brightness using a one-step water vapor-induced phase separation method," *Adv. Funct. Mater.* **29**(23), 1808885 (2019).
16. E. Pini et al., "Diffusion of light in structurally anisotropic media with uniaxial symmetry," *Phys. Rev. Res.* **6**(2), 023051 (2024).
17. J. Heino et al., "Anisotropic effects in highly scattering media," *Phys. Rev. E* **68**(3), 031908 (2003).
18. A. Kienle, "Anisotropic light diffusion: an oxymoron?" *Phys. Rev. Lett.* **98**(21), 218104 (2007).
19. E. Alerstam, "Anisotropic diffusive transport: connecting microscopic scattering and macroscopic transport properties," *Phys. Rev. E* **89**(6), 063202 (2014).
20. R. Vasques and E. W. Larsen, "Non-classical particle transport with angular-dependent path-length distributions. II: Application to pebble bed reactor cores," *Ann. Nucl. Energy* **70**, 301–311 (2014).
21. S. E. Han, "Transport mean free path tensor and anisotropy tensor in anisotropic diffusion equation for optical media," *J. Opt.* **22**(7), 075606 (2020).
22. S. D. Konecky et al., "Imaging scattering orientation with spatial frequency domain imaging," *J. Biomed. Opt.* **16**(12), 126001 (2011).
23. L. Pattelli et al., "Spatio-temporal visualization of light transport in complex photonic structures," *Light: Sci. Appl.* **5**(5), e16090 (2016).
24. L. Pattelli and G. Mazzamuto, "Experimental imaging and Monte Carlo modeling of ultrafast pulse propagation in thin scattering slabs," *J. Biomed. Opt.* **27**(8), 083020 (2022).
25. E. Pini et al., "Breakdown of self-similarity in light transport," arXiv:2304.02773 (2023).
26. P. Naglič et al., "PyXOpto: an open-source python library with utilities for fast light propagation modeling in turbid media," in *Eur. Conf. Biomed. Opt.*, Optica Publishing Group, p. EM3C–2 (2021).
27. H. Wabnitz et al., "Performance assessment of time-domain optical brain imagers, part 1: basic instrumental performance protocol," *J. Biomed. Opt.* **19**(8), 086010 (2014).
28. J. Carlsson et al., "Time-resolved studies of light propagation in paper," *Appl. Opt.* **34**(9), 1528–1535 (1995).
29. P. M. Johnson and A. Lagendijk, "Optical anisotropic diffusion: new model systems and theoretical modeling," *J. Biomed. Opt.* **14**(5), 054036 (2009).
30. A. Badon et al., "Spatio-temporal imaging of light transport in highly scattering media under white light illumination," *Optica* **3**(11), 1160–1166 (2016).
31. A. Lakhtakia, B. Michel, and W. S. Weiglhofer, "Bruggeman formalism for two models of uniaxial composite media: dielectric properties," *Compos. Sci. Technol.* **57**(2), 185–196 (1997).
32. T. Linder and T. Löfqvist, "Anisotropic light propagation in paper," *Nordic Pulp Pap. Res. J.* **27**(2), 500–506 (2012).
33. T. Linder et al., "Lateral light scattering in fibrous media," *Opt. Express* **21**(6), 7835–7840 (2013).
34. T. Linder et al., "Light scattering in fibrous media with different degrees of in-plane fiber alignment," *Opt. Express* **22**(14), 16829–16840 (2014).
35. D. Modrić, S. Bolanča, and R. Beuc, "Monte Carlo modeling of light scattering in paper," *J. Imaging Sci. Technol.* **53**(2), 20201 (2009).
36. L. G. Coppel, M. Neuman, and P. Edström, "Lateral light scattering in paper: MTF simulation and measurement," *Opt. Express* **19**(25), 25181–25187 (2011).
37. G. Marquez et al., "Anisotropy in the absorption and scattering spectra of chicken breast tissue," *Appl. Opt.* **37**(4), 798–804 (1998).
38. M. F. Wood, X. Guo, and I. A. Vitkin, "Polarized light propagation in multiply scattering media exhibiting both linear birefringence and optical activity: Monte Carlo model and experimental methodology," *J. Biomed. Opt.* **12**(1), 014029 (2007).
39. P. Sun and H. Sun, "Determination of the anisotropy complex refractive indices of chicken tissues *in vitro* at 650 nm," *J. Eur. Opt. Soc.-Rapid Publ.* **5**, 10030 (2010).
40. V. V. Tuchin, "Polarized light interaction with tissues," *J. Biomed. Opt.* **21**(7), 071114 (2016).
41. P. Ghassemi et al., "A new approach for optical assessment of directional anisotropy in turbid media," *J. Biophotonics* **9**(1–2), 100–108 (2016).
42. D. S. Wiersma et al., "Time-resolved anisotropic multiple light scattering in nematic liquid crystals," *Phys. Rev. Lett.* **83**(21), 4321 (1999).
43. A. Mertelj and M. Čopič, "Anisotropic diffusion of light in polymer dispersed liquid crystals," *Phys. Rev. E* **75**(1), 011705 (2007).
44. K. M. Hebeda et al., "Light propagation in the brain depends on nerve fiber orientation," *Neurosurgery* **35**(4), 720–724 (1994).
45. J. Heiskala et al., "Modeling anisotropic light propagation in a realistic model of the human head," *Appl. Opt.* **44**(11), 2049–2057 (2005).
46. M. Azimipour et al., "Extraction of optical properties and prediction of light distribution in rat brain tissue," *J. Biomed. Opt.* **19**(7), 075001 (2014).
47. A. Kienle et al., "Light propagation in dentin: influence of microstructure on anisotropy," *Phys. Med. Biol.* **48**(2), N7 (2002).
48. C. J. Zoller et al., "Parallelized Monte Carlo software to efficiently simulate the light propagation in arbitrarily shaped objects and aligned scattering media," *J. Biomed. Opt.* **23**(6), 065004 (2018).
49. X. U. Zhang et al., "Effect of probe pressure on skin tissue optical properties measurement using multi-diameter single fiber reflectance spectroscopy," *J. Phys.: Photonics* **2**(3), 034008 (2020).
50. I. Ahmed, M. Ali, and H. Butt, "Investigating the influence of probe pressure on human skin using diffusive reflection spectroscopy," *Micromachines* **14**(10), 1955 (2023).
51. C. D. Mobley et al., "Modeling light propagation in sea ice," *IEEE Trans. Geosci. Remote Sens.* **36**(5), 1743–1749 (1998).
52. C. Katlein, M. Nicolaus, and C. Petrich, "The anisotropic scattering coefficient of sea ice," *J. Geophys. Res.: Oceans* **119**(2), 842–855 (2014).
53. D. Modrić, K. P. Maretić, and A. Hladnik, "Determination of point-spread function of paper substrate based on light-scattering simulation," *Appl. Opt.* **53**(33), 7854–7862 (2014).
54. G. Rogers et al., "Measurement of the diffusion of light within paper," *J. Opt. Soc. Amer. A* **36**(4), 636–640 (2019).
55. B. Judkewitz et al., "Translation correlations in anisotropically scattering media," *Nat. Phys.* **11**(8), 684–689 (2015).

Ernesto Pini has been a PhD student at the European Laboratory for Non-Linear Spectroscopy since 2021. His PhD is funded by SONY Europe B.V., and it is conducted in collaboration with their research center in Stuttgart. He received his BS and MS degrees in physics from the University of Florence in 2018 and 2021, respectively. His current research concerns light transport in disordered materials, encompassing interests in photonic materials, biophotonics, and transport theory. He is a member of SPIE.

Biographies of the other authors are not available.